Proceedings of ICES2006
ASME Internal Combustion Engine Division 2006 Spring Technical Conference
May 8-10, 2006, Aachen, Germany

ICES2006-1444

EXHAUST SYSTEM GAS-DYNAMICS IN INTERNAL COMBUSTION ENGINES

R Pearson / Lotus Engineering **M Bassett / Lotus Engineering**

P Virr / Renault F1 Team **S Lever / Renault F1 Team** **A Early / Renault F1 Team**

ABSTRACT

The sensitivity of engine performance to gas-dynamic phenomena in the exhaust system has been known for around 100 years but is still relatively poorly understood. The nonlinearity of the wave-propagation behaviour renders simple empirical approaches ineffective, even in a single-cylinder engine. The adoption of analytical tools such as engine-cycle-simulation codes has enabled greater understanding of the tuning mechanisms but for multi-cylinder engines has required the development of accurate models for pipe junctions. The present work examines the propagation of pressure waves through pipe junctions using shock-tube rigs in order to validate a computational model. Following this the effects of exhaust-system gas dynamics on engine performance are discussed using the results from an engine-cycle-simulation program based on the equations of one-dimensional compressible fluid flow.

NOMENCLATURE

a	speed of sound
c	propagation speed
p	pressure
u	particle speed
κ	ratio of speed heats

Subscripts

0	conditions in undisturbed gas

INTRODUCTION

Literature dealing with the effects of gas-dynamic phenomena in the exhaust manifolds of internal combustion engines dates from the beginning of the twentieth century [1]. Farmer [2], however, mentions work undertaken in 1893 by 'Atkinson and Crossley' which established that the performance of a four-stroke engine is sensitive to the length of its exhaust pipe. Farmer [2] clearly delineates the basic mechanism of 'tuning' the exhaust systems of two-stroke engines. In particular the tuning of the 'self-induction engine'[1] is explained where the aim is to size the length of the exhaust pipe such that the rarefaction wave, generated by the reflection of the blowdown pulse at the open end of the pipe, returns to the exhaust port during the intake and exhaust port overlap period. This is also the basic tuning mechanism for four-stroke engines. Figure 1 was generated using the Lotus Engine Simulation cycle-simulation program, running the single-cylinder engine shown at 7000 rev/min. It can be seen that, for this well-tuned case, the blowdown pulse propagates down the exhaust runner from the exhaust valve (which is at 0mm) and reflects at the open end (at 650mm) to form a deep low-pressure region at the exhaust valve about 180 degrees later in the cycle. The variation of the pressure in the exhaust runner as a function of time and position in the pipe can be seen.

Morrison [3,4] discusses pressure pulsations in the exhaust systems of four-stroke engines and states that engine performance is more sensitive to the pressure at the exhaust valve during the valve overlap period than the level of exhaust back-pressure[2]; manifolds for four- and six-cylinder engines are also discussed. Other workers investigated exhaust system gas dynamics via measurement techniques [5-7] but, by the 1950's, calculation of pressure wave phenomena in exhaust systems was being attempted [8-11]. Modelling techniques progressed rapidly in the 1960's and 70's [11-14] and by the late 1980's commercial software was beginning to be used for engine performance prediction, including the effects of exhaust system design. Today the use of computer simulation is a routine part of the engine design and development process [15,16].

[1] An engine which does not use an auxiliary air pump.

[2] Exhaust back-pressure is the mean pressure level at a point in the exhaust system – in this case in the exhaust port

The design of exhaust silencers has a direct effect on the back-pressure in the exhaust system through pressure-loss effects and this impacts directly on the engine pumping work, as well as the scavenging process in the cylinders. The design of the exhaust manifold also impacts upon the pumping work performed by the engine [17,18] via its influence on the pressure level at the exhaust valve during the exhaust process. In particular the pumping work is most sensitive to the cylinder pressure around the point of mid-piston stroke as the rate of change of cylinder volume is greatest at this point. This is not the motivation of the present work, which is concerned primarily with wave propagation phenomena and their effect on the cylinder scavenging process.

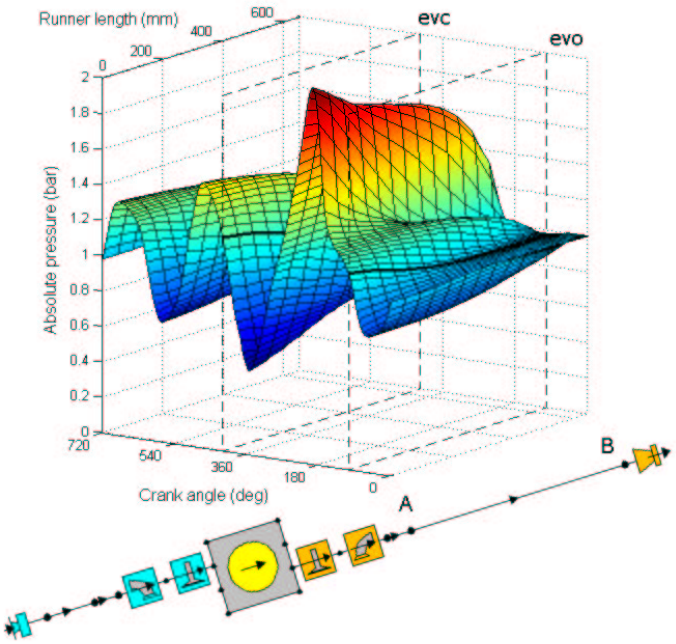

Figure 1. Variation of pressure / crank angle with distance along exhaust pipe at 7000 rev/min.

VALIDATION OF JUNCTION MODELS

A key aspect of the successful simulation of high-performance engines is the ability to predict accurately the propagation of pressure waves through pipe junctions in the exhaust manifold. In this section the accuracy of one- and multi-dimensional models of pipe junctions is assessed. The angular displacement, with respect to each other, of the pipes forming the junction affects the magnitude of the transmitted and reflected waves which are incident upon it. Other characteristics of the junction, for example the way the pipe ends are profiled to form it, also affect the transmission and reflection characteristics but are governed by multi-dimensional features which cannot be resolved using a one-dimensional model.

Three-Pipe Junction

Central to the rig is the modular junction capable of generating 'T-' and 'Y-junctions' of various angular orientations, similar to the types of pipe junction found in the exhaust and intake systems of internal combustion engines. A shock wave is sent down the rig towards the junction and the pressure time history is recorded using piezo-resistive transducers, shown schematically in Figure 2(a). Further details of this rig are given in [19,20]. Figure 2(b) shows the measured pressure / time history at the three different transducer locations from the same test (the repeatability of the experiments was extremely good, as discussed in [20]). The different pressure levels of the transmitted waves through the junction are immediately apparent. The incident shock wave passes transducer P1 and is reflected as a rarefaction wave back into the same pipe. The junction geometry, specifically the different angular disposition of the pipes, causes the transmitted pressure level at location P3 to be significantly higher than the transmitted pressure level at location P2.

Figure 2(c) shows a comparison of measured and predicted pressure / time histories. In this case the predictions are made using the two-dimensional inviscid model described by Batten et al. [21]. It can be seen that the phase and amplitude of the two transmitted waves (P2 and P3) and the reflected wave (P1) are well predicted, and the higher frequency components of the pressure variation are also captured. Examination of a sequence of schlieren images depicting the propagation of the shock front through this junction, presented in [20], shows that these high-frequency oscillations are mostly due to the propagation and reflection of the pressure waves perpendicular to the axis of the pipes.

Figures 2(d) and 2(e) show comparisons of measurements with predictions made using a one-dimensional model (in the work presented in this paper this was Lotus Engine Simulation). It is immediately apparent that the higher frequency components of the pressure / time history are not resolved as a one-dimensional model clearly can only characterise phenomena which vary along the axis of the pipes. The purpose of these models, however, is simply to predict the mean pressure level of the transmitted and reflected waves. The predictions shown in Figure 2(d) were calculated using the 'constant-pressure' model which assumes that the instantaneous pressure level at the end of each pipe forming the junction is equal [16,22]. The predicted pressure levels at transducers P2 and P3 are therefore equal. The pressure level induced by the rarefaction wave at P1 is slightly higher than the levels at P2 and P3. This is because the transducer positions are not coincident at the point of the junction and the velocity level induced by the rarefaction wave differs from that induced by the pressure waves at positions P2 and P3.

The predictions shown in Figure 2(e) are calculated using the generalised pressure-loss junction model described in [22]. This model uses an expression derived from the application of

momentum equations to the junction in order to derive a term for the pressure-loss between any two pipe branches which is used in the boundary equation. The results from this model give an excellent prediction of the mean pressure levels of the transmitted waves. The error in the prediction of the level of the reflected wave at P1 is due to the difficulty of defining an equivalent one-dimensional model which consistently represents the expansion ratio seen by the incident shock wave at the junction.

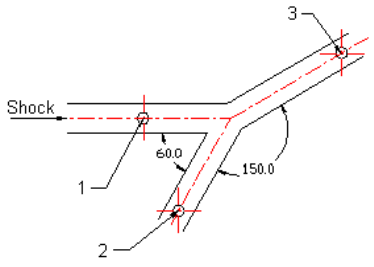

Figure 2(a). Schematic showing geometry and transducer locations of the Y-junction.

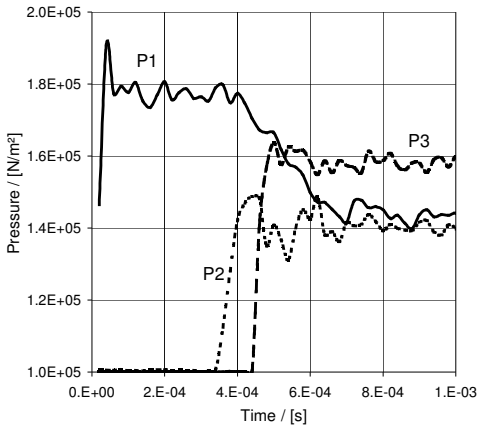

2(b)

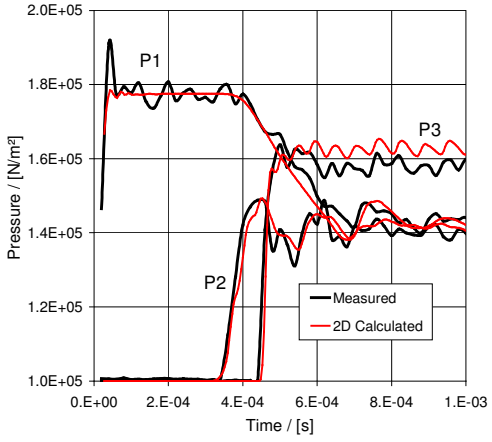

2(c)

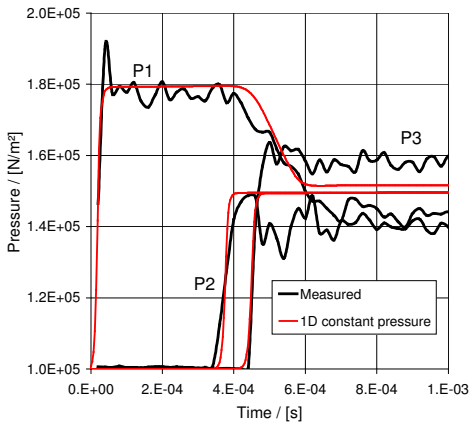

2(d)

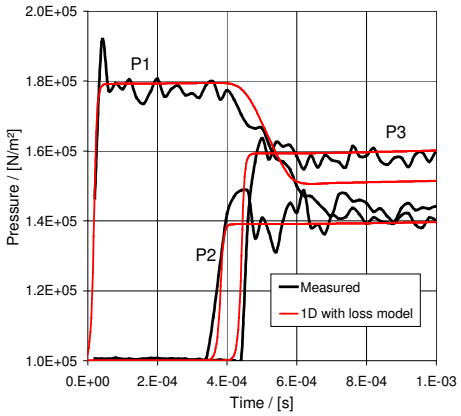

2(e)

Figure 2(b)-(e). Y-junction: comparison of measured and calculated pressures for different models.

Multi-Pipe Junction for Racing Engine

The results discussed in this section were generated from a shock-tube rig using a five-into-one junction, of the type found in the exhaust system of a V10 F1 engine. The rig was designed and built by the authors now affiliated to the Renault F1 Team Engine Division. Figure 3(a) shows the side and end views of the junction tested - the angle between the primary and secondary pipes for this junction is 140 degrees. It is apparent that, in contrast to the junction shown in Figure 2(a), the flow in this junction is three-dimensional in nature. A shock wave is generated by pressurising a short driving tube and then bursting a diaphragm. This wave travels into the junction through one of the exhaust primary runners (Pipe A in Figure 3(a)) and propagates in to the secondary pipe (or tailpipe), seen on the right of the side view of the junction, and into the other exhaust primary runners which have closed ends. The trough in the pressure trace just beyond 0.008 seconds is caused by the rarefaction wave reflected at the junction.

Figure 3(b) shows a comparison of the measured pressure / time history in the incident runner pipe (Pipe A) with results predicted using the one-dimensional model and a three-dimensional CFD code (FLUENT). Both models predict the phase and amplitude of the pressure wave dynamics well. There is a slight discrepancy in the phasing of the one-dimensional results, due to the translation of the junction geometry in to a one-dimensional model. The three-dimensional CFD model, as expected, gives a more accurate prediction of the detailed form of the pressure variation.

Figure 3(c) shows a comparison of measured and predicted pressure variation in pipe B, adjacent to the pipe in which the shock wave was incident upon the junction (pipe A). A much lower amplitude wave than the incident wave propagates into pipe B. Again, both the one-dimensional and three-dimensional models give good predictions of the pressure variation. The simplicity of the former model makes it an extremely efficient approach to incorporating the effects of these complex components in an engine-cycle simulation program.

Figure 4 shows a comparison of measured and predicted power output from a V-10 Formula 1 racing engine fitted with a five-into-one exhaust system of the type shown in Figure 3(a). The exhaust system gas dynamics have a significant effect on the performance of this type of very high-speed engine. The quality of the correlation indicates that the exhaust tuning of the engine is being accurately predicted.

Figure 3(a). Five-into-one junction for F1 engine.

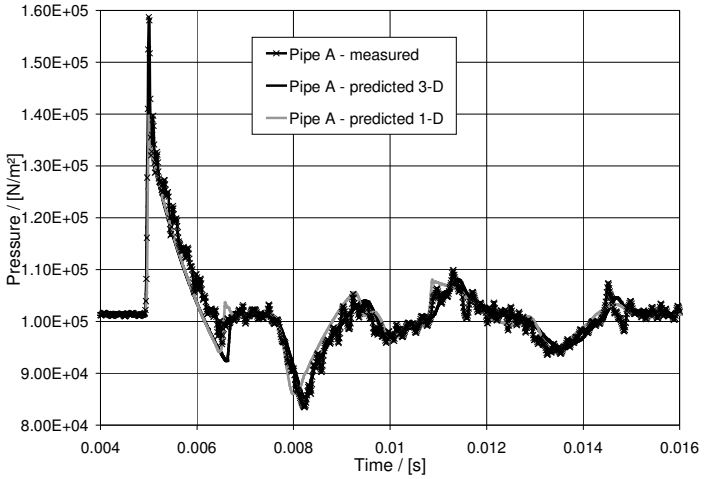

Figure 3(b). Five-into-one junction: measured and predicted pressure variation in pipe A.

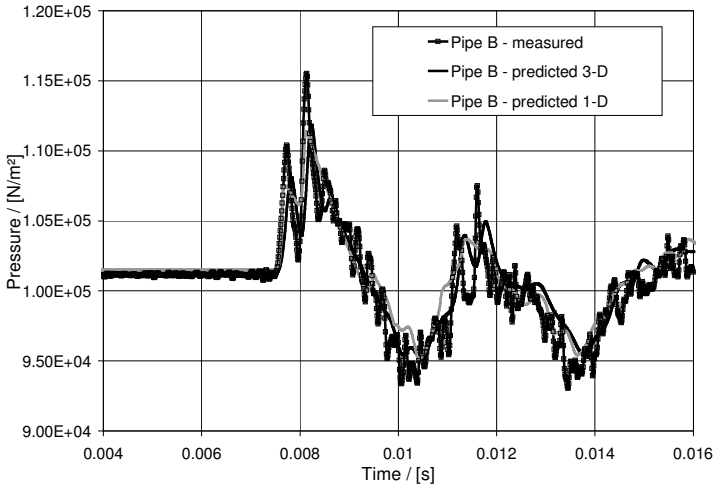

Figure 3(c). Five-into-one junction: measured and predicted pressure variation in pipe B.

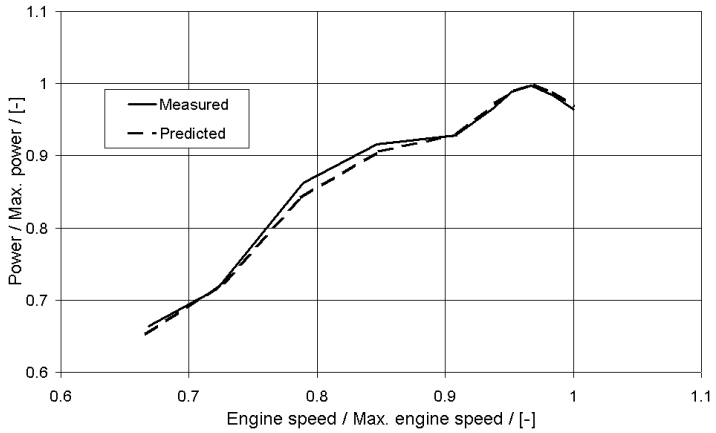

Figure 4. Comparison of measured and predicted power output for V-10 Formula 1 engine.

EMPIRICAL APPROACHES AND THEIR LIMITATIONS

It is common to attempt to calculate the tuned exhaust runner length using analytical methods. The simplest of these approaches involves calculating the time required for a pressure wave to propagate down the exhaust runner and return to the exhaust valve as a rarefaction wave after being reflected at the end of the runner. This apparently straightforward procedure is fraught with difficulty because the propagation speed of the pressure and rarefaction waves differs significantly from the speed of sound in an undisturbed gas. In addition to this, the large particle velocity imparted by the pressure wave delays the return of the rarefaction wave.

Figure 5(a) shows the pressure / crank angle history in the exhaust port (point A) of the 'virtual' high-performance single-cylinder engine shown in Figure 1, at 7000 rev/min. The length of the exhaust pipe and exhaust valve-closing angle are well matched so that a low-pressure level is produced during the valve overlap period. The intake system is also well tuned at this speed. The high pressure at the intake valve opening point (exceeding the cylinder and exhaust port pressures) ensures there is no reverse flow into the intake system. The high pressure in the period after bottom-dead-centre of the induction stroke extends the cylinder charging so that a volumetric efficiency of 122% is achieved.

Simplistic attempts at designing the exhaust system for this engine would usually involve calculating the time for the peak of the blowdown pulse to return to the exhaust valve as the trough of the rarefaction wave. It can be seen in Figure 5 that this period is approximately 170 degrees crank angle, which equates to 4.05×10^{-3} seconds at an engine speed of 7000 rev/min. In this case calculating the time required for a wave to propagate to the end of the pipe and return to the exhaust valve, using a combined port and exhaust runner length of 725 mm and a mean speed of sound of about 690 ms^{-1}(taken from the simulation model), gives 2.10×10^{-3} seconds. Clearly, if used to calculate the optimum pipe length for a particular engine speed, this approach would lead to a large discrepancy with the values predicted by solving the governing equations of one-dimensional gas dynamics in the pipes. The reasons for this discrepancy are discussed below.

Because the waves are nonlinear, the divergences of the speeds of equal amplitude compression and rarefaction waves from the mean speed of sound do not cancel each other out. This can be seen by considering the particle and wave speeds created by pressure and rarefaction waves propagating in an undisturbed gas [16,17,23,24].

The particle velocity induced by the passage of a nonlinear wave is given by

$$u = \frac{2a_0}{\kappa - 1}\left[\left(\frac{p}{p_0}\right)^{\frac{\kappa-1}{2\kappa}} - 1\right] + u_0 \qquad (1)$$

where a_0 and u_0 are the speed of sound and the particle velocity in the undisturbed gas, respectively. The propagation speed, c, of a point on the wave at pressure p is the sum of the local gas velocity and the local speed of sound and is given by

$$c = \frac{2a_0}{\kappa - 1}\left[\frac{(\kappa+1)}{2}\left(\frac{p}{p_0}\right)^{\frac{\kappa-1}{2\kappa}} - 1\right] + u_0 \qquad (2)$$

It can be seen from equation (2) that the propagation speed of points in a wave increase as the pressure increases; this will result in the form of the wave distorting as the high-pressure regions travel faster than the low-pressure regions. For air the value of the ratio of specific heats, κ, is 7/5 and equations (1)-(2) become:

$$u = 5a_0\left[\left(\frac{p}{p_0}\right)^{1/7} - 1\right] + u_0 ;$$

$$c = a_0\left[6\left(\frac{p}{p_0}\right)^{1/7} - 5\right] + u_0 \qquad (3,4)$$

For a point on a non-linear pressure wave where (p/p_0)=1.6 (commonly encountered in both intake and exhaust manifolds) equations (3) and (4) give

$$u = 0.347a_0 + u_0 \quad \text{and} \quad c = 1.417a_0 + u_0 ,$$

showing that the wave propagates into an undisturbed gas (u_0=0) at a speed which is 42 per cent higher than the speed of sound based on the undisturbed gas temperature. The passing of the wave imparts a velocity to the gas molecules of about 35 per cent of the undisturbed speed of sound.

For a point on a rarefaction wave where p/p_0=0.4 (i.e. 0.6 bar below an ambient pressure of 1 bar) equations (3) and (4) give

$$u = -0.613a_0 + u_0 \quad \text{and} \quad c = 0.264a_0 + u_0 ,$$

showing that the wave propagates at a speed which is only 26 per cent of the speed of sound based on the undisturbed gas temperature. The passing of the wave imparts a negative velocity on the gas molecules of about 61 per cent of the undisturbed speed of sound.

When (p/p_0)=0.2791 the propagation speed for non-linear waves (equation (4)) is zero (in air, κ=1.4). The propagation speed becomes negative at pressure ratios less than this value due to the negative particle velocity being greater than the positive propagation speed relative to the gas. In the case of the stationary wave, the gas speed in the backwards direction is just equal to the *local* speed of sound [23].

Having established these principles of nonlinear wave propagation the predicted results shown in Figure 2 from the single-cylinder engine can be re-examined, with a view to discovering why the pressure wave in the exhaust system takes much longer to traverse the exhaust system than a simple calculation would suggest. It is possible to decompose the resultant pressure variation shown in Figure 5(a) in to

component pressure waves which travel in opposite directions [16]. The variation of these component waves during an engine cycle has been plotted in Figures 5(b) and 5(c) at locations A and B in the exhaust system (see Figure 1). In Figure 5(b) it can be seen that the 'forward-travelling' wave (from the exhaust valve to the open end of the pipe) takes about 30 degrees crank angle to travel from point A to point B, shown in Figure 1. The 'reverse-travelling' wave, shown in Figure 5(c), takes approximately 140 degrees crank angle to travel from point B to point A, due to the disproportionately lower propagation speed of the rarefaction wave discussed above. This illustrates the difficulty of using an 'average' speed of sound in order to evaluate exhaust system tuning effects as advocated by some workers [17].

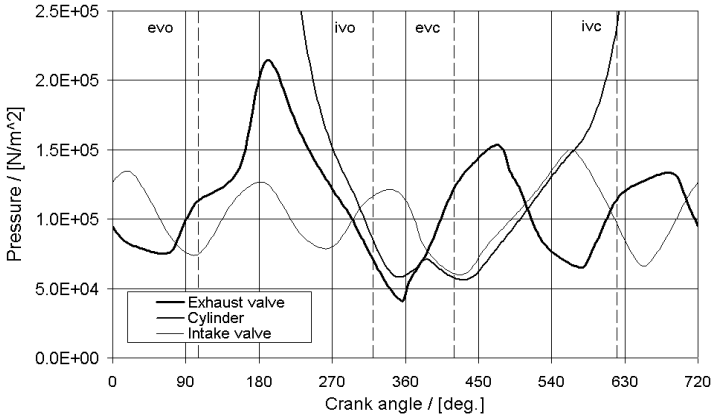

Figure 5(a). Single-cylinder engine: variation of resultant pressure with crank angle at exhaust valve (point A) - 7000 rev/min.

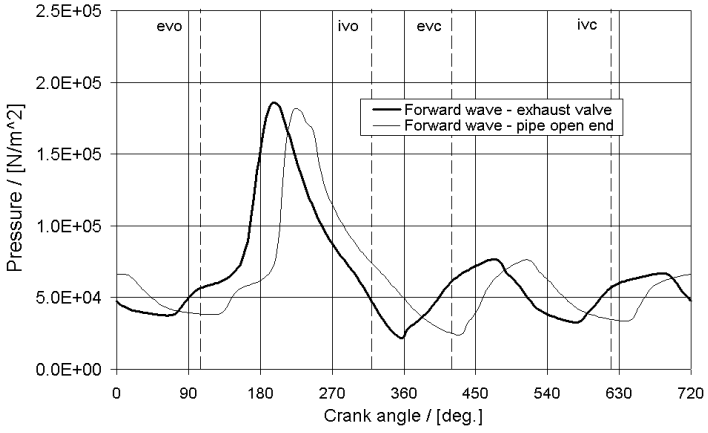

Figure 5(b). Single-cylinder engine: forward-travelling component pressure wave at each end of exhaust pipe – 7000 rev/min.

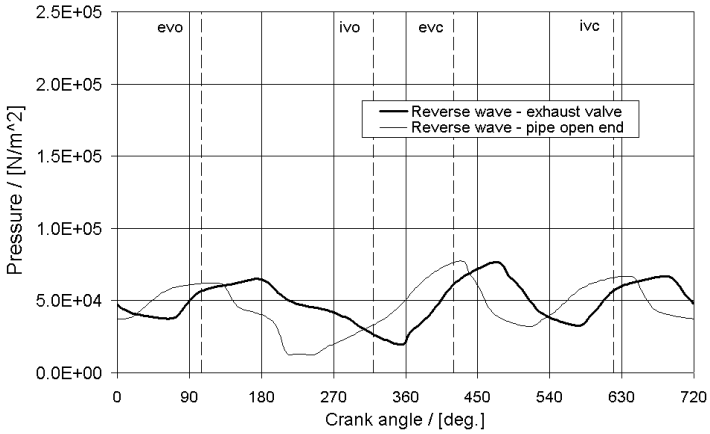

Figure 5(c). Single-cylinder engine: reverse-travelling component pressure wave at each end of exhaust pipe – 7000 rev/min.

SINGLE-CYLINDER ENGINE

The basic tuning of a high-performance single-cylinder engine has been previously discussed [25]. In the present work, only the effects of the exhaust system will be discussed. Figure 6 shows the volumetric efficiency / speed curve for the hypothetical single-cylinder engine shown in Figure 1 with various intake pipe lengths. The heavy line shows the results for the engine fitted with a 650mm exhaust pipe (with 50mm diameter) and a 225mm intake pipe. The resultant and component pressure variation shown in Figures 5(b)-5(d) corresponds to this intake and exhaust system geometry. Figure 6 shows that the underlying shape of the curve is dictated mainly by the intake system whilst Figure 7 shows that the local peaks and troughs are influenced by the design of the exhaust system but that the underlying performance characteristic is not affected.

The cause of the peak at 7000 rev/min has already been discussed and the pressure / time history at the exhaust valve is re-plotted in Figure 8 for the case of the 650mm exhaust pipe. The pressure variation at the exhaust valve at engine speeds of 4500 rev/min and 2500 rev/min are also shown in Figure 8. It can be seen that, at the lower engine speeds, a high pressure level prevails at the exhaust valve during the valve overlap period, which exceeds the amplitude of the pressure in the cylinder and the intake pipe (not shown), causing a reverse flow of residual gas into the intake system. The consequent reduction in the mass of fresh charge the cylinder is able to ingest gives rise to a trough in the volumetric efficiency curve.

Performance optimisation is an iterative process in which the interaction of many parameters is examined. As part of this process the effects of length of the exhaust pipe elements and the timing of the exhaust valve events need to be analysed together. Figure 9 shows how the volumetric efficiency of the engine varies with both exhaust runner length and exhaust-valve-closing (EVC) timing at 2500 rev/min. It is apparent that

maximum volumetric efficiency at this speed is achieved with an exhaust runner length of about 500mm and an exhaust-valve-closing timing of 70 degrees crank angle after top-dead-centre. At other engine speeds the optimum combinations of exhaust pipe length and EVC timing differ.

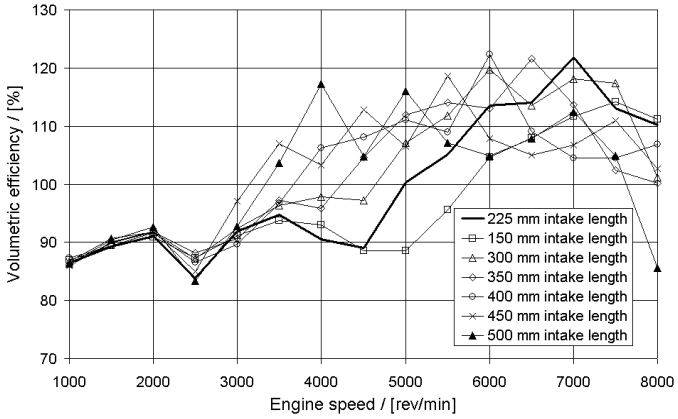

Figure 6. Single-cylinder engine: variation of volumetric efficiency with engine speed for various intake pipe lengths.

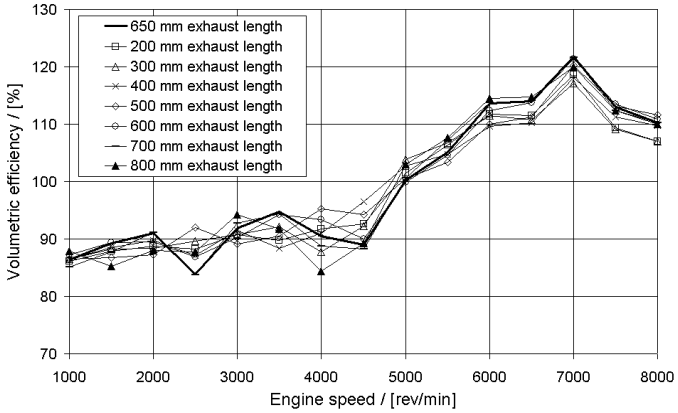

Figure 7. Single-cylinder engine: variation of volumetric efficiency with engine speed for various exhaust pipe lengths.

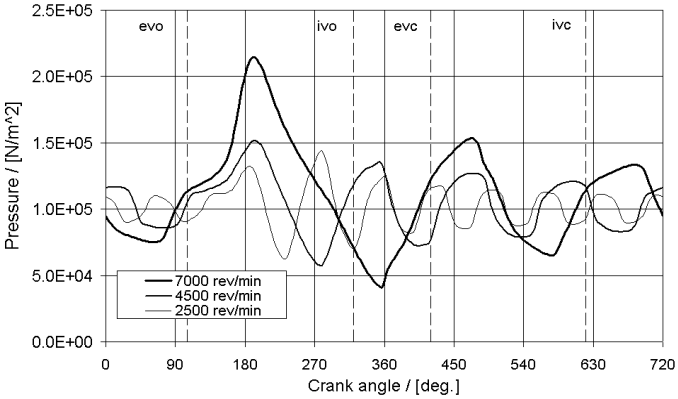

Figure 8. Single-cylinder engine: variation of resultant pressure with crank angle at exhaust valve (point A) for various engine speeds.

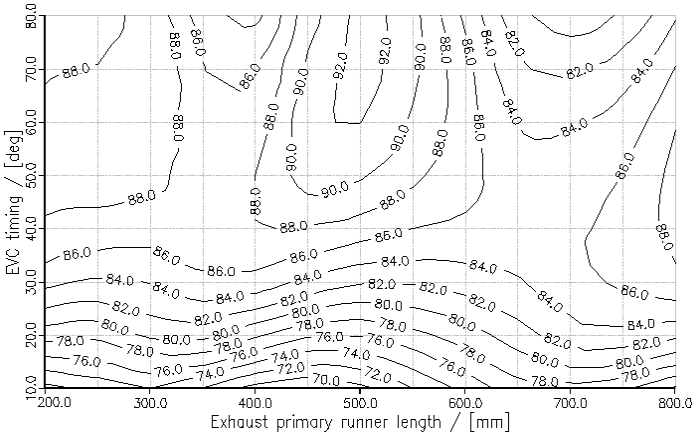

Figure 9. Single-cylinder engine: volumetric efficiency contours as a function of exhaust runner length and exhaust valve closing timing.

TWIN-CYLINDER ENGINE

The tuning mechanisms in exhaust manifolds for multi-cylinder engines are more difficult to understand because of the increased number of sites for generating wave reflections. In this section a twin-cylinder engine is considered in order to provide the simplest type of multi-cylinder manifold. Figure 10(a) shows a model of a twin-cylinder engine based on the 'virtual' single-cylinder engine discussed in Section 4. The firing interval between the two cylinders is 360 degrees crank angle. In this model the exhaust primary runner pipes are identical to that used in the single-cylinder engine model to generate the results shown Figure 5 (i.e. 650mm long, 50mm diameter). These pipes have been joined together to form a 170 degree-Y-junction with a secondary pipe of 60mm diameter. Figure 10(b) shows the sensitivity of the engine volumetric efficiency to the length of the secondary exhaust pipe. In this case, increasing the secondary pipes length generally decreases the performance of the peak volumetric efficiency of the engine but gives benefits at particular points further down the speed range.

The pressure / time history at the exhaust valve at 7000 and 4500 rev/min are shown in Figures 11(a) and 11(b) for secondary pipe lengths of 100mm and 800mm. The pressure / time history for the single-cylinder model discussed in Section 4 is also shown (labelled as 'individual primary pipes' as the result is obviously the equivalent of modelling a twin-cylinder engine with the same exhaust manifold geometry as the single-cylinder engine). It can be seen that connecting the cylinders together with the 100mm secondary pipe gives remarkably similar pressure variation at 7000 rev/min between 90 and 450 degrees crank angle (i.e. for the entire opening duration of the exhaust valve) to that obtained from the single-cylinder engine. At 4500 rev/min the phasing and amplitude of the waves differs somewhat more across the cycle between the single-cylinder engine and the twin-cylinder engine fitted with a 100mm

secondary pipe but the timing of the peak of the pressure wave and the returning rarefaction wave is very similar. For these reasons the volumetric efficiency characteristic of the twin-cylinder engine with the 100mm secondary exhaust pipe and the single-cylinder engine are similar.

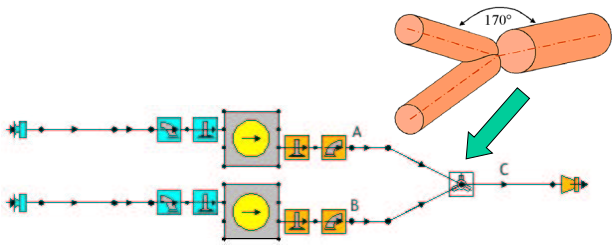

Figure 10(a). Cycle simulation model of twin-cylinder engine.

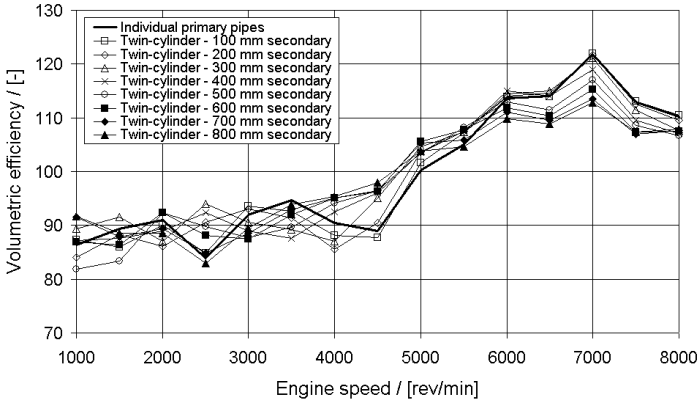

Figure 10(b). Twin-cylinder engine: variation of volumetric with engine speed for various secondary exhaust pipe lengths.

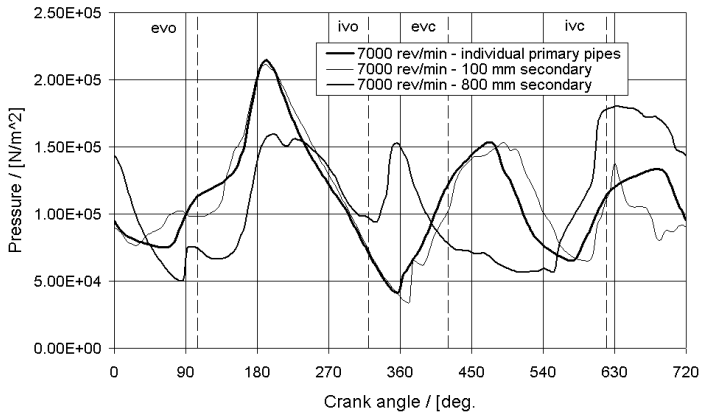

Figure 11(a). Twin-cylinder engine: variation of resultant pressure at the exhaust valve (point A) with crank angle for various secondary pipe lengths – 7000 rev/min.

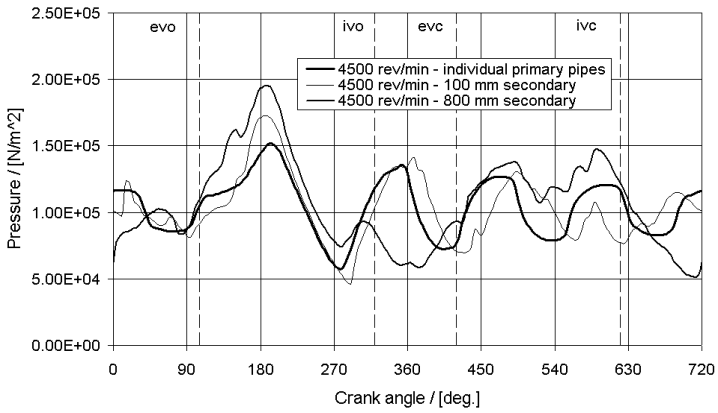

Figure 11(b). Twin-cylinder engine: variation of resultant pressure at the exhaust valve (point A) with crank angle for various secondary pipe lengths – 4500 rev/min.

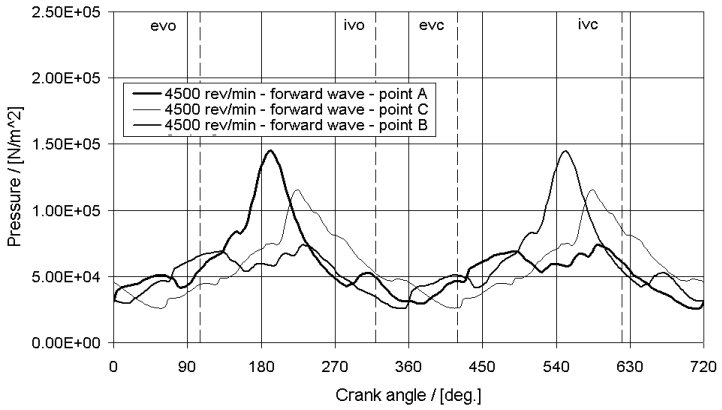

Figure 12(a). Twin-cylinder engine: variation of forward-travelling component pressure waves with crank angle for a secondary pipe length of 800mm – 4500 rev/min.

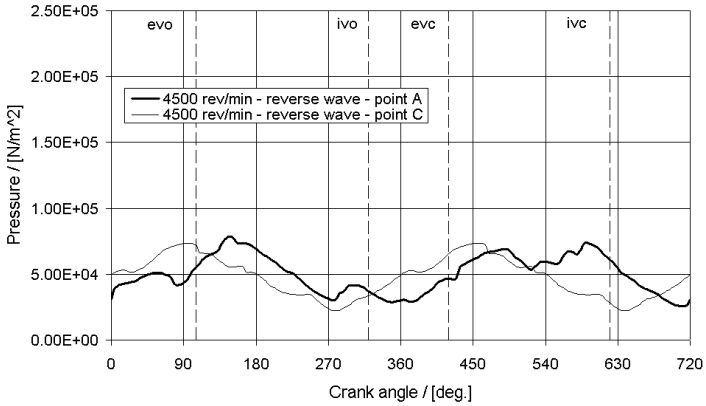

Figure 12(b). Twin-cylinder engine: variation of reverse-travelling component pressure waves with crank angle for a secondary pipe length of 800mm – 4500 rev/min.

When the 800mm secondary pipe is fitted to the twin-cylinder engine the volumetric efficiency of the engine differs significantly from that of the single-cylinder engine. At 7000 rev/min the 800mm secondary pipe produces a high pressure at the exhaust valve in the valve overlap period – this reduces the volumetric efficiency by about nine percentage points. At 4500 rev/min the volumetric efficiency of the twin-cylinder engine fitted with the 800mm secondary pipe is about nine percentage points higher than the single-cylinder engine and ten percentage points higher than the twin-cylinder fitted with the 100mm secondary pipe. The low volumetric efficiency levels are caused by the presence of a high- pressure level at the exhaust valve at the start of the valve-overlap period. With the 800mm secondary pipe a second rarefaction wave arrives to prolong the low pressure created by the reflected blowdown pulse into the valve overlap period.

The origin of this second rarefaction wave can be determined by considering the component pressure waves shown in Figures 12(a) and 12(b). Forward-travelling (left to right) component-pressure waves are shown in Figure 12(a) at points A, B, and C in Figure 10(a). It is clear that the forward-travelling waves initiated at the exhaust valves A and B, at about 200 and 560 degrees crank angle, cause the two peaks in the forward-travelling waves at point C occurring at about 220 and 580 degrees crank angle. The reverse-travelling (right to left) component pressure waves shown in Figure 12(b) indicate that the extension of the low-pressure region in Figure 11(b), for the 800mm secondary pipe, is due to the propagation of the rarefaction wave, created at the end of the secondary pipe, back upstream to the exhaust valve through the junction. It is this mechanism which enhances the volumetric efficiency at 4500 rev/min with the long secondary pipe. A further effect caused by the secondary pipe is that, by propagating and reflecting waves within itself, it modifies the downstream boundary condition for the wave reflection process at the primary pipe.

FOUR-CYLINDER ENGINE

A four-cylinder version of the 'virtual' single-cylinder engine discussed in Section 4 is considered in this section. Again the length of the exhaust primary runner pipes is 650mm. These pipes have been joined together to form a 170 degree four-into-one junction, shown in Figure 13, with a secondary pipe of 70mm diameter. The simulation model is also shown in Figure 13. Figure 14 shows how the volumetric efficiency of the engine varies with the length of the secondary pipe. In this case the secondary pipe appears to have little impact on the peak volumetric efficiency of the engine. This is because the resultant pressure variation at the exhaust port is similar to that of the single-cylinder model (case with individual primary runners) for the range of secondary pipe lengths considered, as shown in Figure 15. This behaviour differs from that of the twin-cylinder engine where the secondary pipe length impacts the engine volumetric efficiency across the speed range. With the four-into-one exhaust manifold the secondary pipe length can be chosen to improve the volumetric efficiency at several of the low-speed operating points (with some options also giving small improvements at the highest engine speeds) without compromising the peak level.

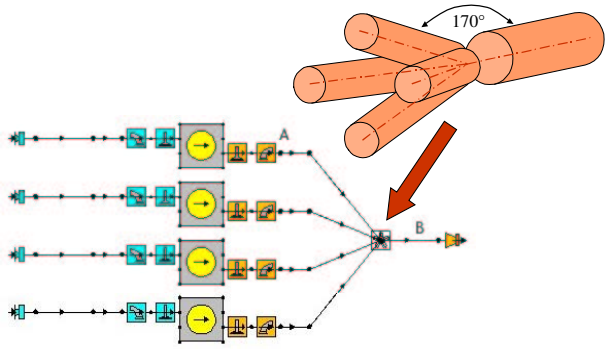

Figure 13. Models of four-cylinder engine: four-into-one exhaust manifold.

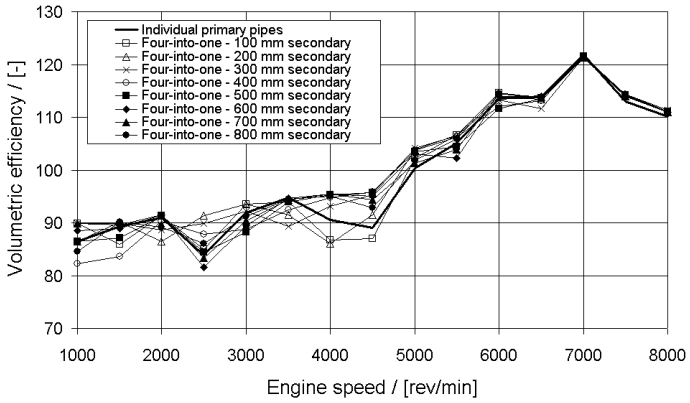

Figure 14. Four-cylinder engine with four-into-one exhaust manifold: variation of volumetric with engine speed for various secondary exhaust pipe lengths.

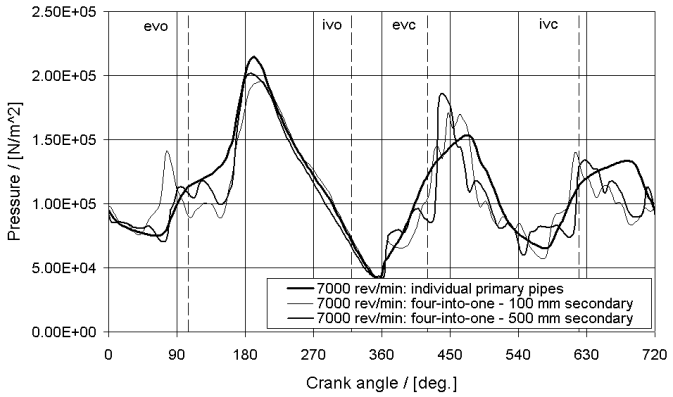

Figure 15. Four-cylinder engine with four-into-one exhaust manifold: variation of pressure with crank angle at the exhaust valve for various secondary exhaust pipe lengths.

CONCLUSIONS

Gas dynamics in the exhaust system of internal combustion engines have a significant effect on their performance. A pressure-loss-junction model, developed by Bassett [20], has been validated for the propagation of pressure waves through both simple Y-junctions and a five-into-one junction of the type used in V10 Formula 1 engines. Simple empirical approaches to designing exhaust systems neglect the large difference in propagation speed of the forward- and reverse-travelling component pressure waves that can lead to large errors in the calculation of tuned lengths. The primary exhaust system tuning mechanism involves producing a low-pressure region during the valve-overlap period. This is achieved by utilising the reflection of the exhaust blowdown pulse at the end of the primary pipe which returns to the valve as a rarefaction wave. In multi-cylinder engines the duration and amplitude of the low-pressure region produced by this rarefaction wave can be increased by the arrival at the exhaust valve of a rarefaction wave that has been created by a reflection process at the end of the secondary pipe. This effect can remove or ameliorate dips in the volumetric efficiency / speed curve and produce benefits in the mid- speed range compared with fitting individual pipes to the cylinders.

REFERENCES

1. Koester, E.W. *Luftkompressoran*. ZVDI, 48, pp. 109-118, 1904.
2. Farmer, H.O. *Exhaust systems of two-stroke engines*. Proc. Instn. Mech. Engrs., 138, pp. 367-390, 1938.
3. Morrison, J.C. *The problem of exhaust silencing and engine efficiency*. Proc. Instn. Auto. Engrs., 27, pp. 614-647, 1932-3.
4. Morrison, J.C. *Exhaust systems for four and six-cylinder engines, with notes on induction and exhaust gas phenomena*. Proc. Instn. Auto. Engrs., 34, pp. 211-252, 1939-40.
5. Mucklow, G.F. *Exhaust-pipe effects in a single-cylinder four-stroke engine*. Proc. Instn. Mech. Engrs., 143, pp. 109-127, 1940.
6. Schweitzer, P.H. *Improving engine performance by exhaust pipe tuning*. J. American Soc. Naval Engnrs., 56, pp. 185-212, 1944.
7. Williams, T.J. *Exhaust arrangements and their influence on the power output of internal-combustion engines*. Proc. Instn. Mech. Engrs., 168, pp. 947-955, 1954.
8. Wallace, F.J., and Mitchell, R.W.S. *Wave action following the sudden release of air through an engine port system*. Proc. Instn. Mech. Engrs., 1B, pp. 343-356, 1952-3.
9. Benson, R.S. *The effect of excess scavenge air on the pressure drop in the cylinder of a two-stroke cycle engine during exhaust blowdown*. J. Roy. Aero. Soc. Tech. Notes, 59, pp. 773-778, 1955.
10. Benson, R.S. *Application of modern gas dynamic theories to exhaust systems of I.C. engines*. Trans. Liverpool Engineering Society, Vol LXXVI, pp.88-112, 1957.
11. Benson, R.S., and Woods, W.A. *Wave action in the exhaust system of a supercharged engine model*. Int. J. Mech. Sci., 1, pp.253-281,1960.
12. Benson, R.S., Garg, R.D., and Woollatt, D. *A numerical solution of unsteady flow problems*. BSRA report no. 375, 1961.
13. Blair, G.P., and Gouldburn, J.R. *The pressure-time history in the exhaust system of a high-speed reciprocating internal combustion engine*. SAE paper no. 670477, 1967.
14. Benson, R.S. *A comprehensive digital computer program to simulate a compression ignition engine including intake and exhaust systems*. SAE paper no. 710773, 1971.
15. Winterbone, D.E. and Pearson, R.J., *Design techniques for engine manifolds – Wave action methods for IC Engines.* Professional Engineering Publications, London, 1999. ISBN 1 86058 179 X.
16. Winterbone, D.E. and Pearson, R.J., *Theory of engine manifold design – Wave action methods for IC Engines.* Professional Engineering Publications, London, 2000. ISBN 1 86058 209 5.
17. Blair, G.P., *Design and simulation of four-stroke engines*. SAE, Warrendale, 1999. ISBN 0-7680-0440-3.
18. Bush, P., Telford, C., Boam, D., and Bingham, J., *A design strategy for four-cylinder SI automotive engine exhaust systems.* SAE paper no. 2000-01-0913, 2000.
19. Bassett, M.D., Pearson, R.J., Winterbone, D.E., and Clough, E., *Visualisation of wave propagation in a three-pipe junction.* I. Mech. E. InternationaI Conference on Optical Methods and Visualisation, City University, London, April 16-17, 1998.
20. Bassett, M.D., *Gas dynamics in the junctions of engine manifolds*. Ph.D. thesis, University of Manchester Institute of Science and Technology, 2003.
21. Batten, P., Lambert, C., and Causon, D., *Positively conservative high-resolution convection schemes for unstructured elements.* Int. J. Num. Meth. Engng., 39, 1821-1838, 1996.
22. Bassett, M.D., Pearson, R.J., Fleming, N.P. and Winterbone, D.E., 'A multi-pipe junction model for one-dimensional, gas-dynamic simulations', SAE Congress and Exposition, Paper No. 2003-01-0370, Detroit, March 3-6, 2003.
23. Earnshaw, S. *On the mathematical theory of sound*. Phil. Trans. Roy. Soc., 150, 133-148, 1860.
24. Bannister, F.K. *Pressure waves in gases in pipes.* Ackroyd Stuart Memorial Lectures, University of Nottingham, 1958.
25. Bassett, M.D., Pearson, R.J., and Fleming, N.P., and O'Brien, M., *Simulating the effects of gas dynamic phenomena on the performance of internal combustion engines.* 8th EAEC Conference, Bratislava, 18th-20th June, 2001.